Published in final edited form as:
Integr Biol (Camb). 2013 March ; 5(3): 481–494. doi:10.1039/c3ib20249f.

Convolution of chemoattractant secretion rate, source density, and receptor desensitization direct diverse migration patterns in leukocytes†

Yana Wang[a] and **Darrell J. Irvine**[b,c,d,*]

[a]Dept. of Chemical Engineering, Massachusetts Institute of Technology, Cambridge, MA 02139, USA

[b]Dept. of Biological Engineering, Dept. of Materials Science & Engineering, Koch Institute for Integrative Cancer Research, Massachusetts Institute of Technology, Cambridge, MA 02139, USA

[c]Ragon Institute of MGH, MIT, and Harvard, Boston, MA 02139, USA

[d]Howard Hughes Medical Institute, Chevy Case, MD 20815, USA

Abstract

Chemoattractants regulate diverse immunological, developmental, and pathological processes, but how cell migration patterns are shaped by attractant production in tissues remains incompletely understood. Using computational modeling and chemokine-releasing microspheres (CRMs), cell-sized attractant-releasing beads, we analyzed leukocyte migration in physiologic gradients of CCL21 or CCL19 produced by beads embedded in 3D collagen gels. Individual T-cells that migrated into contact with CRMs exhibited characteristic highly directional migration to attractant sources independent of their starting position in the gradient (and thus independent of initial gradient strength experienced) but the fraction of responding cells was highly sensitive to position in the gradient. These responses were consistent with modeling calculations assuming a threshold absolute difference in receptor occupancy across individual cells of ~10 receptors required to stimulate chemotaxis. In sustained gradients eliciting low receptor desensitization, attracted T-cells or dendritic cells swarmed around isolated CRMs for hours. With increasing CRM density, overlapping gradients and high attractant concentrations caused a transition from local swarming to transient "hopping" of cells bead to bead. Thus, diverse migration responses observed *in vivo* may be determined by chemoattractant source density and secretion rate, which govern receptor occupancy patterns in nearby cells.

Introduction

Cell motility and guided tissue trafficking are fundamental to diverse processes in development, pathology, homeostasis of the immune system, and responses to infection.[1–5] Host chemokines play a particularly critical role in trafficking of immune cells, by regulating leukocyte interactions with endothelial cells and entry/exit from tissues,[6,7] compartmentalization within lymphoid organs,[8] and promoting chemotactic (directional) or chemokinetic (random) motility.[9–12] Chemoattractant molecules can also be derived from pathogens themselves, promoting recruitment of leukocytes to sites of infection.[13] Within

†Electronic Supplementary Information (ESI) available: Supplementary methods, Supplementary Figures 1–8, and 6 Supplementary Videos. See DOI: 10.1039/b000000x/

Fax: +1-617-452-3293; Tel: +1-617-452-4174; djirvine@mit.edu.

tissues, chemoattractants produced by local cells can diffuse in soluble form and/or bind to the surrounding extracellular matrix, leading to soluble or matrix-bound chemokine fields in the surrounding tissue environment.[14–16] Concentration gradients of such attractants provide spatial cues guiding chemotactic or haptotactic cell migration. The importance of host chemokines to proper functioning of immunity is reflected in the substantial defects in lymphoid organ development[17] and responses to infectious challenge[18] observed in animals genetically deficient in one or more chemoattractants or their receptors. These key roles for chemotaxis in immune function have also motivated interest in potentially engineering chemoattractant responses *in vivo* for therapeutic ends.[19–21]

Chemoattractants stimulate diverse cellular migration responses *in vivo*. Intravital and whole-tissue explant imaging studies have shown that abundant ligands for the chemokine receptor CCR7 stimulate T-cell motility in lymph nodes,[22,23] but migration paths in the lymph node appear largely random, guided by haptokinetic interactions with the chemokine-decorated stromal reticular network.[16,24] Directional migration can also be stimulated by chemoattractants *in vivo*, as has been directly observed for lymph node B-cells migrating toward the T-cell area during immune responses,[10] $CD8^+$ T-cell recruitment to antigen-specific $CD4^+$ T-cell/dendritic cell (DC) pairs in lymph nodes,[12] or neutrophils chemotaxing through tissue to sites of Leishmania infection.[25] “Swarming” behaviours of T-cells aggregating around antigen presenting cells in lymph nodes[26,27] and neutrophils aggregating around parasite-infected cells in skin[25] or lymph nodes[28] have also been described, which likely involve host- or pathogen-derived attractant signals. However, because the nature of the chemoattractant concentration fields in live tissues *in vivo* is typically unknown, the mechanisms by which chemoattractant production, diffusion, matrix binding, and receptor stimulation integrate to elicit such a diversity of responses remain poorly understood.

Few studies have directly visualized chemotactic migration of T-cells or dendritic cells under conditions where the attractant gradient is known/well defined. Current theoretical and experimental evidence suggests that mammalian cell chemotaxis is elicited in the presence of chemoattractant gradients as cells detect ΔR_c, the difference in the number of chemokine-receptor complexes induced at the front vs. rear of the cell.[29–31] Strikingly, the threshold value of ΔR_c required for leukocytes to sense a gradient has been estimated to be as small as ~10 receptors over the length of a cell,[30,32] and very shallow attractant gradients stimulate chemotaxis.[30,33] Recently, microfluidic devices have been developed that permit the generation of stable, linear or near-linear one-dimensional concentration gradients of chemoattractants, in order to expose cells within mm-scale 2D or 3D migration chambers to well-defined attractant stimuli.[34–36] These studies have shown that lymphocytes and DCs are responsive to extremely shallow gradients, and have revealed hierarchies in responsiveness for leukocytes exposed simultaneously to competing gradients.[33,36,37] However, the concentration gradient of attractants formed in proximity to an isolated secreting cell[38,39] or collection of cells[21] is highly nonlinear, with rapid decay in concentration with distance from the secreting source(s). Thus, cells migrating toward a chemokine-releasing cell face both increasing attractant concentration and increasing gradient steepness. Increasing concentrations may suppress the cells’ ability to respond to the gradient through receptor saturation and/or desensitization, while increasing gradient steepness should promote increased directionality to chemotactic migration by increasing the gradient in receptor engagement across the cell body. These two competing effects make it unclear how leukocytes will respond as they approach secreting cells generating physiologically-steep attractant gradients, and whether chemokine signalling alone can promote migration of leukocytes into contact with target secreting cells or temporally-stable retention of cells at a location in space. Microfluidic devices are not well suited to address these problems as they typically create one-dimensional gradients, and do not capture the “point source” nature of individual secreting cells or clusters of cells.

To address these fundamental questions, we employed a reductionist *in vitro* experimental system combined with computational modeling to mimic the production of chemoattractants in tissue and characterize the response of human leukocytes to well-defined locally-produced gradients. We recently designed synthetic hydrogel microspheres with sizes on the order of single cells, which can be loaded with chemokines and release these attractants over a period of many hours at physiologic rates, mimicking secretion by single cells.[40] Here, we embedded these chemokine-releasing microspheres (CRMs) in 3D extracellular matrix gels with human T-cells or DCs, and quantitatively analyzed dynamics of cells responding to gradients of two different chemokines involved in lymphocyte and DC trafficking/homeostasis, CCL19 and CCL21. We found that T-cells migrating into contact with nearby CRMs exhibited highly directional migration independent of their starting position within the attractant gradient, but position in the gradient determined the fraction of T-cells recruited into this responding population. Strikingly, under conditions of low receptor desensitization, stable stimulatory gradients stimulated long-lived swarming of T-cells or DCs around individual attractant-releasing beads. However, high densities of attractant sources, where the ambient attractant concentration is high and neighboring gradients overlap, led to short-lived attraction toward individual sources and biased "hopping" of cells between attractant sources. Together, these results provide substantial insight into how diverse migration responses can be elicited by a single chemokine, depending on the conditions of attractant production in a local tissue.

Results

Physiologic chemokine secretion rates create concentration profiles of CCL19 and CCL21 that stimulate substantial receptor occupancy gradients

To gain a theoretical picture of how chemokine secretion translates into chemoattractant receptor occupancy gradients that direct leukocyte migration, we first modelled the secretion of CCL21 by isolated "source" cells secreting chemokine at a constant rate, and determined the steady-state profile of receptor occupancy for CCR7-expressing cells exposed to this attractant gradient. These initial calculations were made assuming no matrix binding of the chemokine, and considering clearance mechanisms (proteolytic degradation, consumption by non-responding cells, etc.) via a lumped first-order degradation rate constant estimated from experimental measurements of chemokine degradation by serum proteases[41–45] (see Supplementary Methods for detailed transport equations and Table S1, ESI, for summary of model parameters). As illustrated in Fig. S1A, ESI, in the absence of matrix binding, the concentration gradient developed around individual secreting cells releasing chemokine at rates in the physiological range estimated for lymphatic endothelial cells and mature dendritic cells[46–49] reaches steady state within minutes, and thus we subsequently focused on calculation of steady-state gradient characteristics.

The concentration of attractant at a given distance from the source cell determines the fractional occupancy of chemokine receptors on responding CCR7-expressing cells at that location, R_c/R_T (number of attractant-complexed receptors divided by total number of cell surface receptors). The attractant concentration change over the length of a responding cell in turn generates a difference in number of occupied receptors between the front and rear of the cell, the receptor occupancy gradientΔR_c. Both R_c/R_T and ΔR_c have been shown to impact cell migration induced by chemoattractant concentration gradients.[30,33,36] Combined modelling and experimental measurements of ΔR_c have suggested that a threshold difference in receptor occupancy of ~10 receptors is required for leukocytes to sense and respond to attractant gradients.[29,30] Notably, CCR7 is known to be resistant to desensitization by CCL21, which triggers minimal receptor downregulation and elicits sustained stimulation of T-cells, even following hours of exposure to substantial concentrations of ligand.[11,23,50]

Thus, we calculated the chemokine concentration profiles and receptor occupancy gradients of responding cells expressing 10^4 non-desensitizable CCR7 receptors in the vicinity of a source cell secreting CCL21[46–48] (Fig. 1A–B and Fig. S1B, ESI). The secretion rate directly determined both r_{stim}, the maximum distance a functional gradient extended from the cell (assuming a threshold of $\Delta R_c > 10$ receptors over a 10 μm cell body for chemotaxis, Fig. 1C), and the peak strength of the gradient (i.e., maximum ΔR_c and R_c/R_T). Variation of the rate of chemokine clearance rate over a 25-fold range or the number of receptors expressed per cell over a 6-fold range led to modest changes in the predicted receptor occupancy difference generated on responding cells but did not alter the qualitative characteristics of the receptor engagement profiles predicted (data not shown). These calculations lead to several predictions about chemotactic responses in tissues: (1) Receptor saturation is not expected to occur for a responding cell exposed to any of these physiologic chemokine secretion rates, even in close proximity to the secreting cell (Fig. S1B, ESI); (2) higher chemokine secretion rates increase r_{stim}, but this parameter asymptotically approaches a plateau peak value above ~0.5 pg/hr/cell, which limits the maximum distance from the secreting cell that a chemotactic response can be elicited (< 200 μm); and (3) the strength of the chemotactic response (determined by ΔR_c) should increase as responding cells approach the secreting cell, irrespective of the secretion rate.

The qualitative features of these predicted attractant and receptor occupancy profiles remain true if more complex physiologic situations are assumed, though the quantitative details are altered. For example, CCL21 can bind to proteoglycans in the extracellular matrix and on cell surfaces.[9,15,51,52] If secreted chemokine binds to matrix, gradients with qualitatively similar features are formed (irrespective of whether only free soluble attractant is active, only matrix-bound attractant is active, or both soluble and matrix-bound attractant are active, Fig. S1C, ESI).

Also critical to the chemotactic response is the role of receptor internalization and desensitization. Here it is interesting to contrast the two ligands for CCR7: CCL19 and CCL21 bind to CCR7 with comparable affinities (both with estimated K_Ds of several nM,[53–55] but unlike CCL21, CCL19 triggers rapid internalization of CCR7 and desensitization of CCR7 signalling.[50,56,57] We thus next assessed the impact of receptor downregulation and desensitization on the response of leukocytes to a local secreting cell. Using a simple model of ligand-induced receptor desensitization developed by Lin and Butcher[58] (see Supplementary Text, ESI) and desensitization parameters obtained by fitting our own experimental measurements of CCR7 downregulation by CCL19 (Fig. S2, ESI), we calculated the expected receptor occupancy and ΔR_c induced around CCL19-secreting cells. As shown in Fig. 1D, CCL19 in general elicits weaker peak receptor occupancy gradients compared to CCL21 at a given secretion rate. At high CCL19 secretion rates characteristic of dendritic cells,[48] these calculations predict receptor desensitization by CCL19 will lead to a substantially weaker receptor occupancy gradient near the secreting cell compared to an equivalent gradient of CCL21 (~25-fold lower ΔR_c for CCL19 gradients near the source cell).

Chemoattractants are often produced by collections of cells in tissues (e.g., CCL21 produced by stromal cells of inflamed lungs[59] and skin[60] or lymphoid tissues[17,22,23]), and thus we next determined the attractant/CCR7 occupancy gradients that would develop around individual CCL21-secreting cells in a field of uniformly-spaced secreting cells (Fig. 2A), assuming reversible binding of chemokine to matrix, as a function of the density of secreting cells in the tissue. As shown in Fig. 2B, as the density of attractant-secreting cells increases, the steady-state concentration of chemokine and the net fraction of occupied receptors on nearby responding cells increases. In turn, the functional range of the chemokine gradient around each secreting cell contracts as the source cell density increases, irrespective of

whether soluble (Fig. 2C, D), matrix-bound, or both soluble and matrix-bound attractant (not shown) is active. High steady-state concentrations of CCL21 (~150 nM) comparable to the levels experimentally measured in lymph nodes[61–63] are expected for secreting cell densities of ~50 μm between sources. However, even in this setting of dense source cells, the calculations predict locally functional receptor occupancy gradients would exist at short distances (a few cell diameters) around each secreting cell for non-desensitizing binding of CCL21 to CCR7. Thus, responding leukocytes should be capable of sensing local gradients around individual attractant-secreting cells even when high densities of secreting cells are present in a tissue.

Differences in receptor desensitization lead to distinct responsiveness of lymphocytes to CCL21 vs. CCL19 gradients

We next designed an experimental system to mimic CCR7 ligand production in tissue in order to test whether the simple receptor binding/desensitization models employed above correctly predict human leukocyte stimulation by local CCL21 and CCL19 gradients, and to determine the relationship between the magnitude of ΔR_c and actual migration responses. We prepared chemokine-releasing microspheres (CRMs), cell-sized synthetic polysaccharide microspheres that release chemoattractants at tunable rates, to create cell-mimetic CCL19 and CCL21 gradients *in vitro*. CRMs were composed of the polysaccharide alginate, which was loaded with chemokines by adsorption, mimicking the reversible binding of chemokines to polysaccharides in ECM (Fig. S3A–C, ESI).[40] Because fluorophore-conjugated CCL19 and CCL21 were active at concentrations (<5 nM) well below the limits detectable by our fluorescence microscopes (~16 nM), direct visualization of gradients by fluorescence imaging was not possible. Instead, we measured rates of attractant release from collections of microspheres in suspension and used this data combined with the measured size distribution of the microspheres to calculate the expected attractant diffusion profile around individual beads.[40] Though CRMs release embedded chemokine by diffusion of the attractant from the alginate matrix (leading to a decaying release rate with time), the quantity of loaded attractant directly determined the initial release rate and allowed gradients to be generated that modeling predicts are qualitatively very similar to the gradients generated by isolated secreting cells (Fig. S3D–F, ESI). However, the lack of chemokine clearance in this *in vitro* model leads to slow decay of ΔR_c over a period of hours as chemokine builds up in the matrix (Fig. S4, ESI). CCL21-releasing CRMs (CCL21-CRMs) were predicted to drive steadily increasing receptor occupancy gradients with increasing initial release rate, while for CCL19-CRMs, modeling predicted that lack of attractant clearance would elicit pronounced receptor desensitization at higher release rates, giving short-lived gradients and a peak in ΔR_c at intermediate release rates (Fig. 3A, D).

To quantify resting human T-cell responses to these gradients, we measured mean velocities of the cells (v_{mean}) and a hit rate ratio, K_{on}/K_{on}^{rand} measured over 30 min in collagen (Figs. 3B–C, E–F). The hit rate was defined after Castellino et al.[12] as the number of T-cells migrating into contact with an individual CRM per unit time normalized by the total number of cells in the imaging volume (N_{tot}): K_{on} = number of contacts/time•N_{tot}. By taking a ratio of K_{on} to the theoretical hit rate for lymphocytes encountering CRMs by chance during random migration through the matrix, K_{on}^{rand} (see Supplemental Text, ESI), we obtained a convenient measure of the degree of directional migration, with $K_{on}/K_{on}^{rand} > 1$ indicating biased migration toward the chemokine sources.

Consistent with the slightly greater sensitivity of human T-cells to CCL19 compared to CCL21,[50] CCL21-CRMs did not stimulate migration speeds above the basal level of resting T-cells alone in collagen for initial release rates less than ~0.2 pg/hr/bead, while CCL19-

CRMs stimulated migration even at the lowest release rate tested (initial rate 0.01 pg/hr/bead, Fig. 3C). Though migration speeds of T-cells plateaued at ~8 μm/min for higher chemokine release rates in the presence of both CCL19-and CCL21-CRMs, the hit rate ratios showed distinct patterns of chemotactic responses to CCR7 ligand gradients: increasing rates of CCL21 release triggered increasing hit rates of T-cells migrating to nearby beads (Fig. 3B), while the hit rate ratio of T-cells migrating toward CCL19-CRMs peaked at the intermediate chemoattractant release rate of ~0.05 pg/hr/particle (Fig. 3E). As a control, T-cells embedded in collagen with "empty" CRMs in the presence of uniform concentrations of soluble CCL21 or CCL19 migrated with similar velocities but showed a hit rate ratio that was not significantly different from 1, indicating random migration (Fig. 3B–C, E). As expected, T-cell migration toward the attractant sources was dependent on G protein-coupled receptor signalling and CCR7, as treatment of cells with pertussis toxin or blocking anti-CCR7 antibodies dropped the hit rate ratio to ~1 (Fig. S5, ESI). Strikingly, for each chemokine, the magnitude of ΔR_c was strongly correlated with the magnitude of chemotaxis detected (compare Figs. 3A, 3B and Figs. 3D, 3E). Notably, the peak chemotactic responses elicited by optimal CCL19 gradients and CCL21 were comparable, but CCL19 gradients stimulated this peak response at ~10-fold lower ΔR_c values (Fig. 3F), which may reflect the more sensitive engagement of downstream signals by CCL19. These findings suggest that the strength of chemotactic responses to both CCL19 and CCL21 gradients are linked to the magnitude of receptor occupancy differences generated across responding lymphocytes, but that on a per-engaged receptor basis, CCL19 engagement of CCR7 more sensitively drives chemotaxis than CCL21.

Individual T-cells recruited by local gradients are highly chemotactic, with increasing gradient steepness increases the fraction of responding cells

As shown in Fig. 1, the gradient generated by isolated cells secreting chemokine at a constant rate is characterized by a temporally stable but spatially-varying concentration and gradient steepness – both the absolute concentration and the relative slope of the concentration profile increase as the separation between the responding cell and source decrease. Using CRMs to approximate this idealized tissue model, we next analysed single-cell migration responses over 1.5 hr as a function of position in the gradient around single CCL21-CRMs (initial release rates 0.7 pg CCL21/bead/hr) or control beadssurrounded by uniform fields of CCL21. From these imaging data, we calculated the approach angle (angle between the cell's displacement vector and a vector from the cell to the bead), instantaneous chemotaxis index (ICI, distance travelled toward the bead divided by total distance moved in a single time interval), turning angle (angle between subsequent displacement vectors in two sequential time steps), and velocity of each cell at each time-point. When resting T-cells were imaged in collagen in the presence of empty beads and 10 μg/mL soluble CCL21 to stimulate random migration, migration paths of the cells followed persistent random walks distributed around the bead (Fig. 4A and Video S1). By contrast, resting T-cells in the vicinity of CCL21-CRMs chemotaxed from distances up to 200 μm directly into contact with the surfaces of the attractant-releasing beads, with many cells exhibiting highly directional migration paths (Fig. 4A and Video S2). For T-cells responding to CCL21-CRMs, mean values determined for all cell/time-point measurements collected at a given distance from the chemokine source over the 1.5 hr imaging window showed that T-cell velocities and turning angles were only weakly dependent on a cell's position within the gradient, but the mean approach angle steadily decreased and mean ICI increased as the distance to the source decreased (Fig. 4A). Our gradient calculations predicted that for this CCL21 release rate, cells up to ~150 μm away from individual beads would be stimulated to chemotax (Fig. 3C), based on the modelled gradient evolution around individual beads and the calculated receptor occupancy expected from the known K_D of CCL21-CCR7 binding. Although this is only a very indirect estimate, this maximum stimulation distance matched

the experimental ICI data well, suggesting that the threshold requirement of $\Delta R_c \geq 10$ receptors for chemotactic responses assumed in the calculations is reasonably accurate. We also analysed the migration response of activated human T-cells, to determine whether primed T-cells with high constitutive motility exhibit similar chemotactic responses to CCL21 at the single-cell level. Human T-cells activated *in vitro* with PHA and IL-2 retained CCR7 expression identical to resting T-cells (not shown). Interestingly, activated T-cells responded more strongly than resting cells to CCL21 gradients, with higher ICI values and lower approach angles achieved at all positions in the local gradient (Fig. 4A).

We were struck by the nearly linear paths followed by many of the T-cells migrating into contact with CCL21-releasing CRMs, some of which began at distances of a more than 100 μm away from the attractant source (Fig. S6, ESI). To better understand this chemotactic response, we calculated the mean percentage of time that individual cells were “highly chemotactic” (HC), defined as the percentage of time-steps where an individual cell had an ICI > 0.5, as a function of their starting position in the gradient. Cells migrating in uniform fields of CCL21 near empty CRMs showed a mean % time HC of ~0.36 (not statistically different from the expected mean value of 0.33 for completely random migration), and this mean value did not vary to significantly with starting distance from the bead (Fig. 4B). In contrast, T-cells migrating in the vicinity of CCL21-CRMs showed a steadily increasing % time HC as their starting distance from the bead decreased; cells within 50 μm of the bead at the start were highly chemotactic for 80% of the observation period. Notably, when this analysis was performed specifically on attracted T-cells (those cells that migrated into contact with the attractant source during the experiment), attracted cells showed a % time HC of 0.75–0.8 independent of their starting distance from the CRM (Fig. 4B dashed line). However, the fraction of attracted cells among all T-cells starting at a given distance from the attractant source increased as the starting separation from the bead decreased (Fig. 4C). These results indicate that attracted cells are made up of a population that commits strongly to the gradient independent of their starting position (and therefore, independent of the magnitude of their initial receptor occupancy gradient); increasing gradient steepness near to the source does not increase the chemotactic prowess of individual recruited T-cells, but does increase the fraction of T-cells that join this highly chemotactic population. Further work will be needed to determine the source of the increasing responding population with increasing gradient strength; this might reflect selective recruitment of T-cells with the highest levels of CCR7 expression at low gradient strength with cells expressing lower levels of receptor engaged by stronger gradients.

Persistent localized gradients of CCL21 induce swarming of attracted leukocytes

Although chemotactic cell migration is commonly assayed over short durations of 30–60 minutes,[64] leukocytes are exposed to persistent attractant sources *in vivo* (e.g., lymphatic endothelial cells and lymphoid stromal cells constitutively producing CCR7 ligands[8,65]), which could stimulate cells over much longer durations. We thus next asked how the migration response of lymphocytes to persistent CCR7 ligand gradients evolves over time, by imaging resting T-cell migration for 6 hrs near isolated CRMs loaded with 7.5 μg CCL21/mg alginate, a loading calculated to produce functional gradients of CCL21 for many hours (Fig. S4A, ESI). Strikingly, within 90 min of mixing T-cells and CCL21-releasing CRMs in collagen, the strong chemotactic response led the vast majority of cells to accumulate around the nearest attractant microsphere (Fig. 5A), leading to ~80% of cells in a given field of view to be accumulated around beads by the end of 90 min. This accumulation reflected persistent “swarming” of attracted lymphocytes around individual CRMs, where cells that reached a CCL21-releasing bead maintained a high velocity but their direction remained pinned at the bead surface over many hours (Fig. 5B and Video S3, ESI). Swarming required a gradient of attractant, as no accumulation was observed when

cells were mixed with beads in uniform concentrations of CCL21 or when attractant was absent (Fig. 5B and data not shown). By labelling a fraction of the cells, we could follow individual cells swarming at beads and found that the mean retention time of individual T-cells around a CCL21-releasing CRM was ~3 hrs, though strikingly, a population of lymphocytes (~10%) were attracted to beads and remained localized at a single attractant source for the duration of the imaging experiment (6 hrs, Fig. 5C). Those T-cells that did begin migrating away from the surface of a CCL21-releasing bead were efficiently "recaptured" by the gradient, with ~80% of cells that began migrating away from the attractant source (against the gradient) over the first 3 hrs turning and migrating back to the bead surface, reaching a median distance from the bead of only ~50 μm before returning to the nearby CCL21 source (Fig. 5D–E).

As expected from the gradient and receptor desensitization calculations, in contrast to CCL21, CRM-generated CCL19 gradients were completely unable to support sustained accumulation of lymphocytes (Video S4, ESI). Using CRMs releasing CCL19 at rates that elicited the peak chemotactic response in short term assays (1 μg CCL19 loaded per mg alginate), T-cells were observed to transiently chemotax toward CCL19 sources over ~30 min, but then migrated away in random directions at later times (Fig. 5A), and though T-cell motility remained high, a significant "trapped" population failed to develop around CCL19-releasing CRMs (Fig. 5B–D). Similar results with even weaker initial chemotaxis were observed at higher and lower CCL19 release rates (not shown).

To determine if the ability of CCL21 gradients to support localized swarming was specific to T-cells or rather a general property of CCL21-CCR7 signalling, we also characterized the migration response of CCR7-expressing LPS-matured human monocyte-derived dendritic cells to both gradients. As shown in Fig. S7 and Video S5, ESI, human DCs expressing CCR7 exhibited stable accumulation and swarming around CCL21 gradient-generating CRMs.). Altogether, these data suggest that sustained chemokine secretion is capable of promoting both prolonged attraction of responding leukocytes and dramatic confinement of attracted cells near the attractant source, provided that receptor desensitization and the steady-state gradient properties permit an above-threshold ΔR_c to be maintained over time.

Ambient chemokine concentration regulates T-cell chemotaxis through changes in receptor occupancy gradients

The model calculations and results above indicate that isolated persistent chemoattractant sources can elicit very localized sequestration of lymphocytes in the absence of chemokine receptor desensitization. However, as the ambient steady-state concentration of chemoattractant increases in the local microenvironment, the increase in overall receptor occupancy will stimulate chemokinesis in competition with directional migration responses. To determine the impact of the absolute level of chemokine in the local environment on chemotactic responses induced by local gradients, we systematically varied total chemokine levels by adding increasing concentrations of free CCL21 to the collagen matrix along with CCL21-releasing beads. We first calculated the expected gradient around CCL21-CRMs as a function of increasing levels of free attractant pre-existing in the matrix. As illustrated in Fig. 6A and Fig. S8A–C, ESI, at any given timepoint as the background concentration of free attractant increases, receptor occupancy increases at all points in the gradient, and the receptor occupancy gradientΔR_c steadily decreases. However, the calculations predict that for ambient concentrations of free CCL21 up to 10 nM (100 ng/mL), ~2-fold above the K_D of CCL21-CCR7 binding, T-cells should still be capable of chemotaxing when they come within ~50 μm of a CCL21-releasing bead for several hours (Fig. 6A; Fig. S8C, ESI).

Experimentally, resting T-cells mixed with CCL21-CRMs together with varying concentrations of free CCL21 showed similar velocities irrespective of the level of free

CCL21 present (Fig. S8D, ESI). However, the hit rate ratio for T-cells encountering CRMs dropped monotonically as the concentration of free CCL21 increased, reaching the hit rate expected for completely random migration at 1 μg/mL background CCL21 (Fig. 6B). Analysis of the ICI of T-cells migrating near CCL21-releasing beads over a 30 min period showed a contraction in both the maximum distance from an CRM where chemotaxis was triggered and the magnitude of the chemotactic index achieved as the concentration of free attractant in the matrix increased (Fig. 6C): Chemotaxis was detected within 50 μm of CCL21-CRMs in the presence of 100 ng/mL free CCL21, but no attraction was detected for 1 μg/mL free CCL21. Analysis of the fraction of T-cells trapped by CRM gradients showed that T-cell swarming persisted in the presence of low levels of background attractant (10 ng/mL free CCL21), but the fraction of cells localized at the bead surfaces dropped as the ambient CCL21 concentration was increased (Fig. 6D–E). Interestingly, activated T-cells responded to CCL21 concentration gradients more sensitively than resting T-cells, retaining persistent (> 60 min) swarming responses to CRM-generated gradients in the presence of 25-fold higher background CCL21 levels (Fig. 6E). Thus, T-cells can detect local gradients of CCL21 produced by nearby cells even in the presence of substantial background levels of free attractant in the local microenvironment.

Overlapping CCL21 gradients trigger a transition from “swarming” around isolated attractant sources to “hopping” between local gradients

Our calculations of gradient formation suggest that even in tissues with high densities of secreting cells (such as primary and secondary lymphoid organs), local gradients around individual source cells should lead to chemotaxis-inducing receptor occupancy differences in nearby lymphocytes (Fig. 2). However, as the density of attractant-secreting cells in a tissue increases, the sharp gradients produced within 100–200 μm of individual cells will begin to overlap. At such high densities of attractant-secreting cells (as expected for example in lymph nodes), lymphocytes migrating even a few cell diameters away from one source will detect the increasing gradient from another nearby source, which might lead to transient, sequential chemotactic responses as cells move from source to source. Alternatively, high overall receptor occupancy achieved in this setting might elicit an overwhelming chemokinetic signal triggering unbiased, random migration. To determine which of these situations prevails, we varied the mean separation between CCL21-releasing CRMs dispersed stochastically in collagen. Using CCL21-CRMs that triggered peak chemotaxis for isolated beads (7.5 μg CCL21 loaded per mg alginate), we measured the response of T-cells to several different densities of CCL21 sources, starting from a maximum separation of 500 μm between sources.

As before, we first calculated the expected concentration profiles and receptor occupancy profiles as a function of the separation distance between beads. Over short times of 30–60 min, CRMs as close as 100 μm apart were predicted to induce stimulatory ΔR_c values in responding cells, but only within a few cell diameters of the source (Fig. S9, ESI), qualitatively similar to the situation predicted for dense chemokine sources in tissue (Fig. 2). We next imaged T-cells mixed in collagen with dense CCL21-releasing CRMs, limiting the imaging time to the first 60 min, as buildup of chemokine in our *in vitro* model system was predicted to cause rapid decay of ΔR_c over a period of several hours (Fig. S9, ESI). As shown in Fig. 7A, hit rate ratios measured for T-cells in the presence of CCL21-releasing CRMs were highest when beads were separated by the largest distances, and ambient chemokine concentration and overlap between neighboring gradients was lowest. K_{on}/K_{on}^{rand} was statistically greater than 1 even for the closest bead separation tested (70 μm average distance between CRMs). However, as expected from our “ambient” chemokine experiments, T-cells did not exhibit prolonged swarming around individual attractant sources, as the retention time of T-cells around individual CRMs was only ~15 min for

beads separated by 200 μm and decayed to only ~5 min for CRMs separated by 70 μm (Fig. 7B). Rather, resting T-cells interspersed transient migration near individual beads with biased paths hopping bead to bead (Fig. 7C). The combination of biased migration near CRMs with short retention times around any single chemokine source led to a substantial increase in the number of sources "visited" by individual T-cells in a given interval of time as the CRM density increased (Fig. 7D). Thus, the ability of T-cells to transiently respond to local gradients in chemokine-rich tissues may provide an effective mechanism to increase the scanning of cells for antigen.

Finally, we also compared the migration behavior of PHA+IL-2-activated T-cells in this dense-source setting. Strikingly, activated T-cells show a much greater sensitivity to the short range gradients formed around individual CCL21-CRMs at high density in the collagen matrix. As shown in Fig. 8A and Video S6, ESI, Even CCL21-CRMs separated by only a few cell diameters accumulated their own "private" clusters of swarming T-cells, which showed a much lower frequency of hopping among beads compared to resting T-cells. This is illustrated by the plots of the fraction of trapped T-cells in Fig. 8B, where each CRM is shown to stably trap a fraction of the surrounding T-cells, in a manner which is sustained over > 2 hr. Thus, even in the setting of dense attractant point sources as might be expected in lymphoid organs, activated T-cells show distinct chemoattraction behavior compared to naïve/resting T-cells that could have functional consequences *in vivo*.

Discussion

Here we have used a reductionist model for chemokine production in tissue combined with computational analyses to systemically study how qualitative and quantitative features of chemokine gradients generated by attractant-secreting cells influence leukocyte migration at the single-cell level. We focused on responses triggered by signalling through the CCR7 chemokine receptor, in part because of the importance of CCR7 signalling in guiding leukocyte migration into and within primary and secondary lymphoid organs,[66,67] and also because the two ligands for CCR7, CCL19 and CCL21, exhibit distinct intracellular signalling and receptor desensitization responses despite similar binding affinities,[50,56,57,68] providing an experimental test-bed to ask how chemotactic responses elicited by the same receptor are altered by the presence or absence of strong desensitization.

Prior experimental studies of chemotaxis using classical Dunn chambers or more recently developed microfluidic devices designed to expose cells to well-defined chemoattractant gradients have estimated that neutrophils exhibit directional migration in response to minimum receptor occupancy differences of ~10 receptors over the length of the cell.[30,32] This threshold appears to also hold for human T-cells responding to CCL21 and CCL19 gradients, as our experimental data was well described by gradient modelling employing this minimum value of ΔR_c as a threshold for chemotactic responses. Using this threshold for functional responses, our computational analysis predicted maximum stimulatory distances for chemotactic responses to isolated secreting cells of ~150 μm, in good agreement with the experimental data and similar to calculated maximum distances of paracrine communication predicted for individual cytokine-producing cells in tissue.[38] Interestingly however, we found that the relationship between the input signal (ΔR_c) and the output response (chemotaxis) differed for CCL19 and CCL21 gradients, with CCL19 stimulating equivalent chemotactic responses at 10-fold weaker ΔR_c inputs. This may reflect enhanced downstream signalling induced by CCL19, which is much more potent at inducing phosphorylation of ERK1/2 than CCL21.[57]

Although rates of T-cells migrating into contact with chemoattractant-releasing beads were directly correlated with the magnitude of the receptor occupancy gradient induced in nearby

cells, we found that interestingly, those cells that migrated into contact with the attractant sources characteristically exhibited highly-directed migration, irrespective of their initial position in the gradient. Increasing hit rates with increasing gradient strength reflected an increasing fraction of T-cells recruited into this highly chemotactic population.

Though in many traditional *in vitro* assays (e.g., modified Boyden-chamber experiments) CCL19 and CCL21 elicit similar chemotaxis from T-cells, we show here in this more physiologic model of localized gradient formation that these two ligands for CCR7 can elicit extremely different biological responses. T-cells were only transiently responsive to CCL19 and quickly lost directionality in CRM-generated gradients, irrespective of the chemokine release rate employed (Fig. 5 and data not shown). In contrast, CCL21-CRMs were capable of stimulating sustained swarming of T-cells around individual sources, localizing the position of the cells within a roughly 100 μm-diameter space for many hours provided the release rate was sufficient to generate a stimulatory gradient (Fig. 5). These results are consistent with predictions from our simple models of CCL19 and CCL21 signalling, which predicted pronounced receptor desensitization by CCL19 but sustained receptor occupancy gradients in responding T-cells migrating within CCL21 gradients. These findings add to previously reported differences in the ability of CCL19 and CCL21 to stimulate dendritic cell chemotaxis due to differences in matrix binding, observed in microfluidic devices.[33] We also found sustained chemoattraction of activated T-cells toward CRMs with another chemokine/receptor pair (CXCL10 binding CXCR3, data not shown), which exhibits receptor desensitization intermediate between CCL19 and CCL21, suggesting such localized swarming responses are not unique to CCL21 triggering of CCR7.

If above-threshold ΔR_c values always induced chemotaxis and subsequent “trapping” as shown above for isolated attractant sources, T-cells would be very inefficient at scanning APCs in lymphoid microenvironments; this is counter to the known rapid scanning behavior of T-cells in lymph nodes at steady state.[69] However, attractant-secreting stromal cells are present at high densities in secondary lymphoid organs, and steady-state chemokine levels of 2–10 μg/mL have been estimated in lymph nodes.[61–63] Notably however, even in such chemokine-rich environments, modelling predicts that chemokines eliciting low or no desensitization (such as CCL21) will still induce a stimulatory receptor occupancy gradient within a few cell diameters of individual secreting cells. Experimentally, this led to a transition from swarming to “hopping” of resting T-cells between attractant sources as the source density increased, with short residence times near individual attractant sources. Such locally biased migration may be part of enhancing the efficiency of T-cell-DC encounters *in vivo*. It is possible that biased organization of collagen fibers at the surface of individual beads influences the migration paths of cells at the surface of beads, but these effects would be the same in both the “swarming” and “hopping” experiments, and thus the attractant gradients present appear to play a dominant role in the observed migration responses. Interestingly, we found that activated T-cells showed an ability respond with highly localized swarming around individual attractant sources even when CRMs were placed at high density, indicating a high responsiveness to receptor occupancy gradients even when the absolute fraction of engaged receptors is very high. Exploring the biochemical mechanisms underlying this response is an area for future studies, but may have significant implications for accumulation of primed T-cells at sites of infection or responses to localized infections in lymph nodes.[70]

In summary, our studies provide evidence that human T-cells and dendritic cells exhibit chemotactic responses to CCR7 ligands governed by a threshold requirement for receptor occupancy differences of ~10 receptors over the length of the cells, in good agreement with earlier estimates made for neutrophils.[30,32] In the presence of local point sources, chemotactic responses of T-cells are heavily influenced by the source density and receptor

desensitization, with low receptor desensitization promoting prolonged residence times of cells around individual sources. These findings indicate that attempts to engineer chemotaxis for therapeutic ends (e.g., in vaccines, regenerative medicine, or cancer therapy) will likely be most effective using chemokines such as CCL21 that trigger low levels of receptor desensitization, to enable recruited cells to be stably accumulated at a target tissue site. The data also suggest that diverse migration responses can be elicited from any given chemokine/receptor pair depending on the quantitative details of gradient generation, and explain how striking swarming behaviours observed in some settings *in vivo* can be achieved even by soluble attractant gradients.

Materials and Methods

Modelling of chemokine gradient profiles

The concentration of chemokine (C) evolving around spherical source cells or beads 20 μm in diam. releasing attractant were computationally modeled using commercial COMSOL Multiphysics finite element modeling software (COMSOL Inc., Burlington, MA) and solving the diffusion equation:

$$\frac{\partial C}{\partial t} = D\nabla^2 C - R_p - R_M$$

where D is the chemokine diffusion constant, R_p is the rate of chemokine clearance, and R_M accounts for reversible chemokine binding to the matrix (see Supplemental Text and Table S1, ESI, for complete details and parameter values employed). Cells were modeled as sources releasing attractant at a constant rate, while CRMs were modeled as releasing attractant by diffusion through the alginate matrix starting from a constant initial concentration of attractant within the microsphere at time zero. The diffusion constant for chemokine diffusion through the alginate matrix of each bead was determined from experimental measurements of chemokine release as previously described.[40] Calculations were performed assuming either periodic boundary conditions (mimicking a finite density of secreting sources regularly arrayed in space, as in Fig. 2) or assuming isolated sources in an infinite space (Fig. 1 calculations). Receptor occupancy gradients were calculated from the attractant concentration profiles by assuming equilibrium between receptor and ligand in the environment, and receptor desensitization was modeled using the approach of Lin and Butcher[58] (see Supplemental Text, ESI).

Cells

Peripheral blood mononuclear cells (PBMCs) were isolated by ficoll gradients from unpurified buffycoats of healthy anonymous donors (Research Blood Components, Boston, MA). Resting T-cells were isolated by magnetic sorting (pan human T-cell negative selection kit, Miltenyi, Auburn, CA) and cultured in RPMI-glutamax (Invitrogen, Carlsbad, CA) containing 10 mM HEPES and 10% fetal calf serum (FCS) for 18 hr prior to use. Activated T-cells were prepared by stimulating PBMCs with 1 μg/ml PHA for 2 days. On day 3, stimulated PBMCS were ficolled to remove dead cells, followed by magnetic sorting of T-cells and culture for 1 day with 100 U/ml IL-2 (Chiron, Emeryville, CA) before use on day 4. To prepare dendritic cells (DCs), monocytes were isolated from PBMCs by magnetic selection (CD14 positive selection kit, Miltenyi) and cultured with 25 ng/ml IL-4 (Peprotech, Rocky Hill, NJ) and 100 ng/ml GM-CSF (R&D systems, Minneapolis, MN) for 7 d to generate monocyte-derived DCs. Medium was changed every other day; on day 5, 100 ng/ml LPS was added to mature the DCs, and the cells were used for experiments on day 7.

Cells used for imaging were labeled with 2.5 μM CMTPX tracer dye (Invitrogen) prior to experiments according to the manufacturer's instructions.

Videomicroscopy chemotaxis assay

Alginate bead CRMs with a mean size of ~30 μm diam. were prepared and loaded with chemokine by adsorption from concentrated attractant solutions just before use as previously described.[40] For some experiments, 1% Alexafluor 488-conjugated chemokine was included to fluorescently mark the CRMs. Soluble collagen (*PureCol*® bovine type I collagen, Advanced Biomatrix, Tucson, AZ ~3 mg/ml stock acid solution) was mixed with 0.1 M sterile NaOH and 10X phenol red-free RPMI medium in an 8:1:1 vol ratio to achieve pH 7.2, then combined with FCS (final conc. 10% vol/vol) and phenol red-free RPMI at a ratio of 3:0.33:0.67 to obtain a final collagen concentration of 1.8 mg/ml. Collagen solution mixed with CMTPX-labeled cells (final conc. 3×10^6 cells/ml) and chemokine-loaded CRMs was deposited into pre-heated chambered coverglasses (Nalge Nunc Labtek, Rochester, NY) and immediately placed in a 5% CO_2, 37°C humidified environmental chamber on a Zeiss Axiovert 200 inverted fluorescence microscope. Fields of view containing single or multiple CRMs were selected and imaged in time-lapse at 20X. A brightfield image and an 80 μm red fluorescence *z*-stack with 4.2 μm *z*-step size was collected every 1 min (5 min for DCs) for up to 10 hrs. 80 μm *z*-stack green fluorescence images were taken before and after time-lapses to indicate the location of the CRM microspheres.

Single-cell migration analysis

Single cell migration paths from the imaging data were tracked in 3D for the time window indicated in the text using Volocity 5.2 (PerkinElmer, Waltham, MA). The hit rate, K_{on}, was defined as the number of T-cells migrating into contact with a particle per unit time normalized by the total number of cells in the imaging volume N_{tot}:[12]

$$K_{on}=\frac{number\,of\,contacts}{time\cdot N_{tot}}$$

By taking a ratio of K_{on} to the theoretical hit rate for lymphocytes encountering CRMs by chance during random migration through the matrix, K_{on}^{rand}, we obtained a convenient measure of the degree of directional migration, with $K_{on}/K_{on}^{rand} > 1$ indicating biased migration toward the chemokine sources. K_{on}^{rand} was calculated using a simple 3D random collision model as previously derived:[71]

$$K_{on}^{rand}=\pi(r_T+r_M)^2 v_T$$

where r_T is the radius of the CRM, r_M is the contact radius of a cell touching the CRM surface (15 μm) and v_T is the average velocity of the cells.

As further measures characterizing cell migration responses, we calculated: (i) velocity of the cells; (ii) approach angle, the angle between a vector from the cell to the nearest CRM and the vector of cell movement at a given time step, (0o for a cell moving directly along the gradient, 90o perpendicular to the gradient and 180o perfectly antiparallel to the gradient); (iii) turning angle, the angle between subsequent displacement vectors from two sequential time steps; and (iv) The instantaneous chemotactic index (ICI), defined as the displacement of each cell in the direction of the attractant gradient divided by the total path length traveled over a single observation interval (1 min for T-cells and 5 min for DCs).[40,72] ICI values of 1

reflect migration vectors perfectly aligned with the attractant gradient and -1 perfectly antiparallel to the gradient; mean values of zero reflect completely random migration. To capture the effect of differences in the chemoattractant gradient as a function of distance from the bead, these parameters were binned in 25 μm intervals of distance of the cell from the bead and the values within each bin were averaged to capture the mean strength of chemotaxis as a function of position in the gradient over the analysis time: i.e. we averaged all the values collected for cells 0–25 μm from the CRM, 25–50 μm away, 50–75 μm away, etc. Cells whose starting positions were beyond 200 μm were binned together and labeled 250 μm. For analysis of beads at higher densities (Figs. 7 and 8), cell paths were analyzed around clusters of beads that distributed within the collagen gels at approximately uniform spacing, to account for the lack of precise control on bead spacing. Analyses of cells swarming around microspheres that departed and were “recaptured” by the gradient were conducted using Image J (NIH, Bethesda, MD).

Statistical analysis

Measured values are expressed as means ± standard errors (SE). Levels of significance for comparing groups were using two-tailed nonparametric t-tests. All calculations were made using GraphPad Prism 5.0.

Supplementary Material

Refer to Web version on PubMed Central for supplementary material.

Acknowledgments

This work was supported in part by the NIH (EB007280). DJI is an investigator of the Howard Hughes Medical Institute.

References

1. Mackay CR. Moving targets: cell migration inhibitors as new anti-inflammatory therapies. Nature Immunology. 2008; 9:988–998. [PubMed: 18711436]
2. Kondo S, Miura T. Reaction-diffusion model as a framework for understanding biological pattern formation. Science. 2010; 329:1616–1620. [PubMed: 20929839]
3. von Andrian UH, Mempel TR. Homing and cellular traffic in lymph nodes. Nat Rev Immunol. 2003; 3:867–878. [PubMed: 14668803]
4. Friedl P, Weigelin B. Interstitial leukocyte migration and immune function. Nature immunology. 2008; 9:960–969. [PubMed: 18711433]
5. Shields JD, et al. Autologous chemotaxis as a mechanism of tumor cell homing to lymphatics via interstitial flow and autocrine CCR7 signaling. Cancer Cell. 2007; 11:526–538. [PubMed: 17560334]
6. Debes GF, et al. Chemokine receptor CCR7 required for T lymphocyte exit from peripheral tissues. Nature immunology. 2005; 6:889–894. [PubMed: 16116468]
7. Bao X, et al. Endothelial heparan sulfate controls chemokine presentation in recruitment of lymphocytes and dendritic cells to lymph nodes. Immunity. 2010; 33:817–829. [PubMed: 21093315]
8. Cyster JG. Chemokines, sphingosine-1-phosphate, and cell migration in secondary lymphoid organs. Annu Rev Immunol. 2005; 23:127–159. [PubMed: 15771568]
9. Woolf E, et al. Lymph node chemokines promote sustained T lymphocyte motility without triggering stable integrin adhesiveness in the absence of shear forces. Nature immunology. 2007; 8:1076–1085. [PubMed: 17721537]
10. Okada T, et al. Antigen-engaged B cells undergo chemotaxis toward the T zone and form motile conjugates with helper T cells. PLoS Biol. 2005; 3:e150. [PubMed: 15857154]

11. Stachowiak AN, Wang Y, Huang YC, Irvine DJ. Homeostatic lymphoid chemokines synergize with adhesion ligands to trigger T and B lymphocyte chemokinesis. J Immunol. 2006; 177:2340–2348. [PubMed: 16887995]
12. Castellino F, et al. Chemokines enhance immunity by guiding naive CD8+ T cells to sites of CD4+ T cell-dendritic cell interaction. Nature. 2006; 440:890–895. [PubMed: 16612374]
13. Teixeira MJ, Teixeira CR, Andrade BB, Barral-Netto M, Barral A. Chemokines in host-parasite interactions in leishmaniasis. Trends Parasitol. 2006; 22:32–40. [PubMed: 16310413]
14. Proudfoot AE, et al. Glycosaminoglycan binding and oligomerization are essential for the in vivo activity of certain chemokines. Proc Natl Acad Sci U S A. 2003; 100:1885–1890. [PubMed: 12571364]
15. Patel DD, et al. Chemokines have diverse abilities to form solid phase gradients. Clin Immunol. 2001; 99:43–52. [PubMed: 11286540]
16. Schumann K, et al. Immobilized chemokine fields and soluble chemokine gradients cooperatively shape migration patterns of dendritic cells. Immunity. 2010; 32:703–713. [PubMed: 20471289]
17. Muller G, Hopken UE, Lipp M. The impact of CCR7 and CXCR5 on lymphoid organ development and systemic immunity. Immunological reviews. 2003; 195:117–135. [PubMed: 12969315]
18. Kursar M, et al. Differential requirements for the chemokine receptor CCR7 in T cell activation during Listeria monocytogenes infection. The Journal of experimental medicine. 2005; 201:1447–1457. [PubMed: 15851484]
19. Jhunjhunwala S, et al. Bioinspired Controlled Release of CCL22 Recruits Regulatory T Cells In Vivo. Adv Mater. 2012
20. Tayalia P, Mazur E, Mooney DJ. Controlled architectural and chemotactic studies of 3D cell migration. Biomaterials. 2011; 32:2634–2641. [PubMed: 21237507]
21. Zhao X, Jain S, Benjamin Larman H, Gonzalez S, Irvine DJ. Directed cell migration via chemoattractants released from degradable microspheres. Biomaterials. 2005; 26:5048–5063. [PubMed: 15769541]
22. Okada T, Cyster JG. CC chemokine receptor 7 contributes to Gi-dependent T cell motility in the lymph node. J Immunol. 2007; 178:2973–2978. [PubMed: 17312142]
23. Worbs T, Mempel TR, Bolter J, von Andrian UH, Forster R. CCR7 ligands stimulate the intranodal motility of T lymphocytes in vivo. J Exp Med. 2007; 204:489–495. [PubMed: 17325198]
24. Bajenoff M, et al. Stromal cell networks regulate lymphocyte entry, migration, and territoriality in lymph nodes. Immunity. 2006; 25:989–1001. [PubMed: 17112751]
25. Peters NC, et al. In vivo imaging reveals an essential role for neutrophils in leishmaniasis transmitted by sand flies. Science. 2008; 321:970–974. [PubMed: 18703742]
26. Miller MJ, Wei SH, Parker I, Cahalan MD. Two-photon imaging of lymphocyte motility and antigen response in intact lymph node. Science. 2002; 296:1869–1873. [PubMed: 12016203]
27. Tang Q, et al. Visualizing regulatory T cell control of autoimmune responses in nonobese diabetic mice. Nature immunology. 2006; 7:83–92. [PubMed: 16311599]
28. Chtanova T, et al. Dynamics of neutrophil migration in lymph nodes during infection. Immunity. 2008; 29:487–496. [PubMed: 18718768]
29. Devreotes PN, Zigmond SH. Chemotaxis in eukaryotic cells: a focus on leukocytes and Dictyostelium. Annu Rev Cell Biol. 1988; 4:649–686. [PubMed: 2848555]
30. Herzmark P, et al. Bound attractant at the leading vs. the trailing edge determines chemotactic prowess. Proc Natl Acad Sci U S A. 2007; 104:13349–13354. [PubMed: 17684096]
31. Zigmond SH. Mechanisms of sensing chemical gradients by polymorphonuclear leukocytes. Nature. 1974; 249:450–452. [PubMed: 4834231]
32. Zigmond SH. Consequences of chemotactic peptide receptor modulation for leukocyte orientation. The Journal of cell biology. 1981; 88:644–647. [PubMed: 6260816]
33. Haessler U, Pisano M, Wu M, Swartz MA. Dendritic cell chemotaxis in 3D under defined chemokine gradients reveals differential response to ligands CCL21 and CCL19. Proc Natl Acad Sci U S A. 2011; 108:5614–5619. [PubMed: 21422278]
34. Jeon NL, et al. Neutrophil chemotaxis in linear and complex gradients of interleukin-8 formed in a microfabricated device. Nat Biotechnol. 2002; 20:826–830. [PubMed: 12091913]

35. Irimia D. Microfluidic technologies for temporal perturbations of chemotaxis. Annu Rev Biomed Eng. 2010; 12:259–284. [PubMed: 20450351]
36. Ricart BG, John B, Lee D, Hunter CA, Hammer DA. Dendritic cells distinguish individual chemokine signals through CCR7 and CXCR4. J Immunol. 2011; 186:53–61. [PubMed: 21106854]
37. Lin F, Butcher EC. T cell chemotaxis in a simple microfluidic device. Lab Chip. 2006; 6:1462–1469. [PubMed: 17066171]
38. Francis K, Palsson BO. Effective intercellular communication distances are determined by the relative time constants for cyto/chemokine secretion and diffusion. P Natl Acad Sci USA. 1997; 94:12258–12262.
39. Fleury ME, Boardman KC, Swartz MA. Autologous morphogen gradients by subtle interstitial flow and matrix interactions. Biophys J. 2006; 91:113–121. [PubMed: 16603487]
40. Wang Y, Irvine DJ. Engineering chemoattractant gradients using chemokine-releasing polysaccharide microspheres. Biomaterials. 2011; 32:4903–4913. [PubMed: 21463892]
41. Lambeir AM, et al. Kinetic investigation of chemokine truncation by CD26/dipeptidyl peptidase IV reveals a striking selectivity within the chemokine family. J Biol Chem. 2001; 276:29839–29845. [PubMed: 11390394]
42. Proost P, et al. Proteolytic processing of CXCL11 by CD13/aminopeptidase N impairs CXCR3 and CXCR7 binding and signaling and reduces lymphocyte and endothelial cell migration. Blood. 2007; 110:37–44. [PubMed: 17363734]
43. Tong S, Yuan F. Numerical simulations of angiogenesis in the cornea. Microvasc Res. 2001; 61:14–27. [PubMed: 11162192]
44. Vempati P, Mac Gabhann F, Popel AS. Quantifying the proteolytic release of extracellular matrix-sequestered VEGF with a computational model. PLoS One. 2010; 5:e11860. [PubMed: 20686621]
45. Zabel BA, et al. Chemoattractants, extracellular proteases, and the integrated host defense response. Exp Hematol. 2006; 34:1021–1032. [PubMed: 16863908]
46. Chieppa M, et al. Cross-linking of the mannose receptor on monocyte-derived dendritic cells activates an anti-inflammatory immunosuppressive program. J Immunol. 2003; 171:4552–4560. [PubMed: 14568928]
47. Lebre MC, et al. Differential expression of inflammatory chemokines by Th1- and Th2-cell promoting dendritic cells: a role for different mature dendritic cell populations in attracting appropriate effector cells to peripheral sites of inflammation. Immunol Cell Biol. 2005; 83:525–535. [PubMed: 16174103]
48. Sallusto F, et al. Distinct patterns and kinetics of chemokine production regulate dendritic cell function. Eur J Immunol. 1999; 29:1617–1625. [PubMed: 10359116]
49. Issa A, Le TX, Shoushtari AN, Shields JD, Swartz MA. Vascular endothelial growth factor-C and C-C chemokine receptor 7 in tumor cell-lymphatic cross-talk promote invasive phenotype. Cancer Res. 2009; 69:349–357. [PubMed: 19118020]
50. Bardi G, Lipp M, Baggiolini M, Loetscher P. The T cell chemokine receptor CCR7 is internalized on stimulation with ELC, but not with SLC. Eur J Immunol. 2001; 31:3291–3297. [PubMed: 11745346]
51. Christopherson KW 2nd, Campbell JJ, Travers JB, Hromas RA. Low-molecular-weight heparins inhibit CCL21-induced T cell adhesion and migration. J Pharmacol Exp Ther. 2002; 302:290–295. [PubMed: 12065729]
52. Friedman RS, Jacobelli J, Krummel MF. Surface-bound chemokines capture and prime T cells for synapse formation. Nat Immunol. 2006; 7:1101–1108. [PubMed: 16964261]
53. Willimann K, et al. The chemokine SLC is expressed in T cell areas of lymph nodes and mucosal lymphoid tissues and attracts activated T cells via CCR7. Eur J Immunol. 1998; 28:2025–2034. [PubMed: 9645384]
54. Ott TR, et al. The N-terminal domain of CCL21 reconstitutes high affinity binding, G protein activation, and chemotactic activity, to the C-terminal domain of CCL19. Biochem Biophys Res Commun. 2006; 348:1089–1093. [PubMed: 16904643]

55. Yoshida R, et al. EBI1-ligand chemokine (ELC) attracts a broad spectrum of lymphocytes: activated T cells strongly up-regulate CCR7 and efficiently migrate toward ELC. Int Immunol. 1998; 10:901–910. [PubMed: 9701028]
56. Byers MA, et al. Arrestin 3 mediates endocytosis of CCR7 following ligation of CCL19 but not CCL21. J Immunol. 2008; 181:4723–4732. [PubMed: 18802075]
57. Kohout TA, et al. Differential desensitization, receptor phosphorylation, beta-arrestin recruitment, and ERK1/2 activation by the two endogenous ligands for the CC chemokine receptor 7. J Biol Chem. 2004; 279:23214–23222. [PubMed: 15054093]
58. Lin F, Butcher EC. Modeling the role of homologous receptor desensitization in cell gradient sensing. J Immunol. 2008; 181:8335–8343. [PubMed: 19050250]
59. Lo JC, et al. Differential regulation of CCL21 in lymphoid/nonlymphoid tissues for effectively attracting T cells to peripheral tissues. J Clin Invest. 2003; 112:1495–1505. [PubMed: 14617751]
60. Serra HM, Baena-Cagnani CE, Eberhard Y. Is secondary lymphoid-organ chemokine (SLC/CCL21) much more than a constitutive chemokine? Allergy. 2004; 59:1219–1223. [PubMed: 15461605]
61. Luther SA, et al. Differing activities of homeostatic chemokines CCL19, CCL21, and CXCL12 in lymphocyte and dendritic cell recruitment and lymphoid neogenesis. J Immunol. 2002; 169:424–433. [PubMed: 12077273]
62. Stein JV, et al. The CC chemokine thymus-derived chemotactic agent 4 (TCA-4, secondary lymphoid tissue chemokine, 6Ckine, exodus-2) triggers lymphocyte function-associated antigen 1-mediated arrest of rolling T lymphocytes in peripheral lymph node high endothelial venules. J Exp Med. 2000; 191:61–76. [PubMed: 10620605]
63. Fan L, Reilly CR, Luo Y, Dorf ME, Lo D. Cutting edge: ectopic expression of the chemokine TCA4/SLC is sufficient to trigger lymphoid neogenesis. J Immunol. 2000; 164:3955–3959. [PubMed: 10754285]
64. Wei SH, Parker I, Miller MJ, Cahalan MD. A stochastic view of lymphocyte motility and trafficking within the lymph node. Immunol Rev. 2003; 195:136–159. [PubMed: 12969316]
65. Randolph GJ, Angeli V, Swartz MA. Dendritic-cell trafficking to lymph nodes through lymphatic vessels. Nat Rev Immunol. 2005; 5:617–628. [PubMed: 16056255]
66. Forster R, et al. CCR7 coordinates the primary immune response by establishing functional microenvironments in secondary lymphoid organs. Cell. 1999; 99:23–33. [PubMed: 10520991]
67. Gunn MD, et al. Mice lacking expression of secondary lymphoid organ chemokine have defects in lymphocyte homing and dendritic cell localization. J Exp Med. 1999; 189:451–460. [PubMed: 9927507]
68. Otero C, Groettrup M, Legler DF. Opposite fate of endocytosed CCR7 and its ligands: recycling versus degradation. J Immunol. 2006; 177:2314–2323. [PubMed: 16887992]
69. Miller MJ, Wei SH, Cahalan MD, Parker I. Autonomous T cell trafficking examined in vivo with intravital two-photon microscopy. P Natl Acad Sci USA. 2003; 100:2604–2609.
70. Chtanova T, et al. Dynamics of T Cell, Antigen-Presenting Cell, and Pathogen Interactions during Recall Responses in the Lymph Node. Immunity. 2009; 31:342–355. [PubMed: 19699173]
71. Miller RG, Dunkley M. Quantitative analysis of the 51Cr release cytotoxicity assay for cytotoxic lymphocytes. Cell Immunol. 1974; 14:284–302. [PubMed: 4219591]
72. Moghe PV, Nelson RD, Tranquillo RT. Cytokine-stimulated chemotaxis of human neutrophils in a 3-D conjoined fibrin gel assay. J Immunol Methods. 1995; 180:193–211. [PubMed: 7714334]

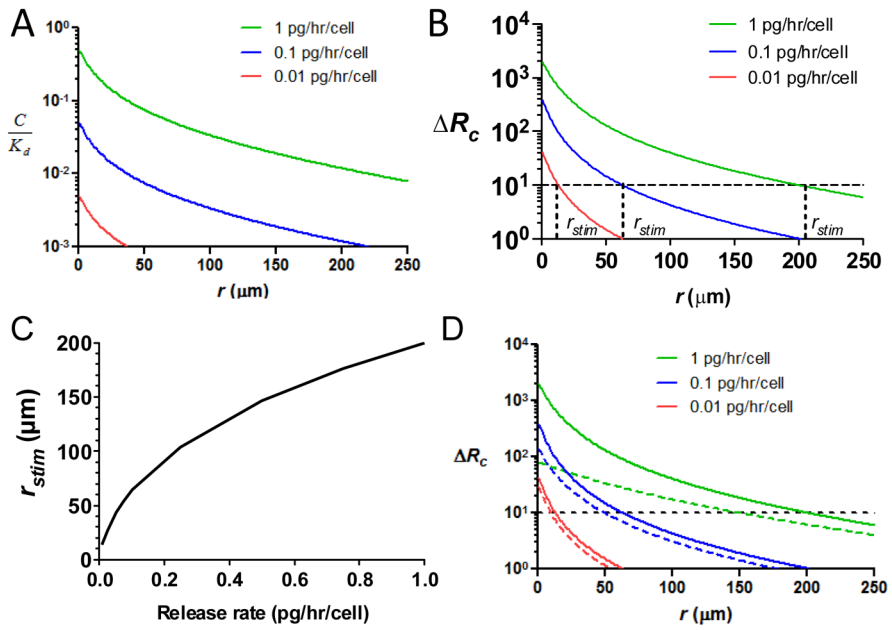

Fig. 1.

Physiological chemokine secretion rates produce steady-state CCL19 or CCL21 gradients that do not saturate responding cell CCR7 receptors and extend up to ~150 μm around individual source cells. Calculations were made of chemoattractant concentration profiles developed as a function of radial distance from the secreting cell surface (at $r = 0$) for isolated secreting cells (20 μm in diameter) releasing CCL21 or CCL19 at a constant rate. Shown are the concentration profiles (A), receptor occupancy difference (B), and maximum stimulation distance r_{stim} (C). (D) Comparison of predicted receptor occupancy gradients for CCL21 (solid lines) vs. CCL19 (dashed lines) for the noted chemokine secretion rates. Horizontal dashed lines in B and D show the estimated threshold level of ΔR_c required for directional migration by responding cells.

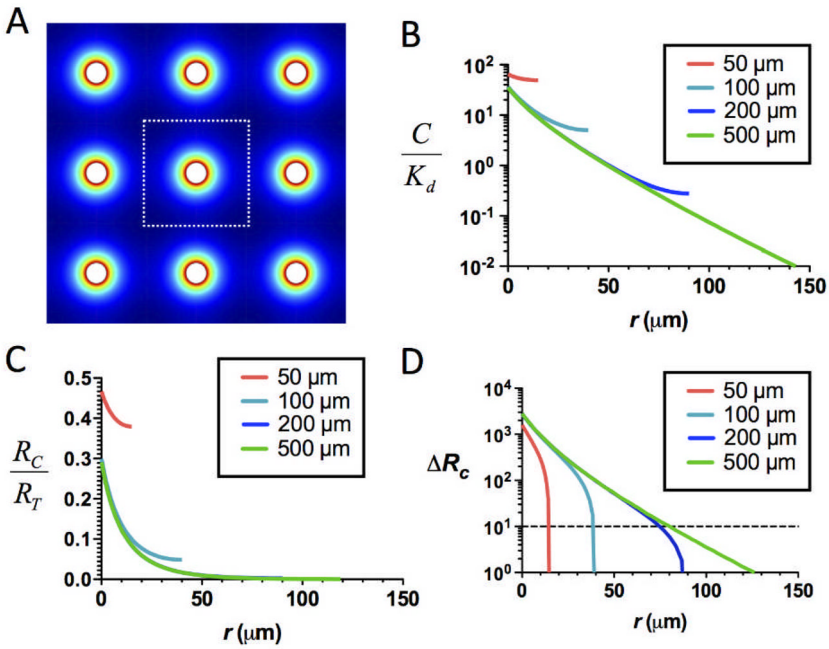

Fig. 2.

Lymphocytes migrating through tissues containing dense arrays of CCL21-secreting cells should still exhibit localized chemotactic responses near each source cell. (A) 2D schematic of FEM model, with a regular array of CCL21 sources (20 μm in diam. with a center-to-center separation of 50–500 μm), showing CCL21 concentration in false color. (B–D) Predicted profiles of normalized total CCL21 concentration (free and matrix-bound, B), receptor occupancy (C), and receptor occupancy difference across responding cells (D) as a function of distance from an individual attractant source in the array, calculated for cells secreting at 1 pg/cell/hr, including matrix binding sites at a density $C_{matrix}/K_m = 10^3$, assuming only CCL21 in solution is active for receptor binding.

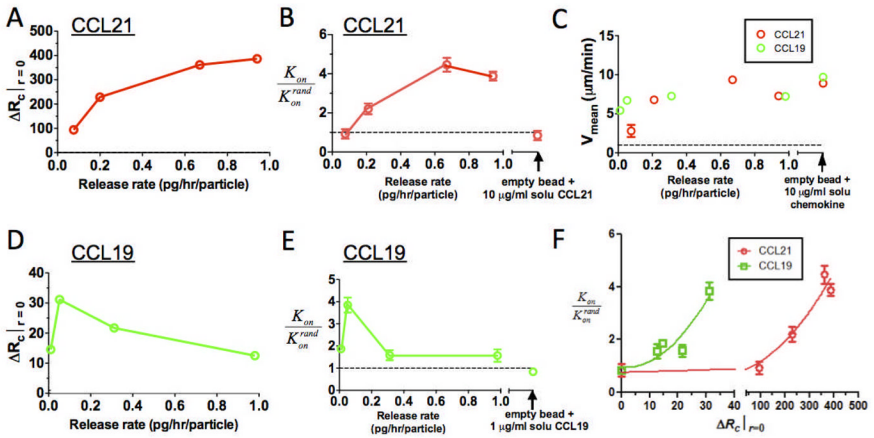

Fig. 3. Receptor occupancy gradients predict human leukocyte chemotactic responses toCCL19 vs. CCL21 attractant gradients

CRMs (releasing CCL19 or CCL21 at the indicated rates) and human resting T-cells were embedded in 3D collagen gels (8×10^3 beads and 3×10^6 cells/cm^3), and T-cell migration responses over 30 min were recorded by videomicroscopy. (A–E) Calculated maximum ΔR_c at the surface of CRMs (A, D), hit rate (K_{on}/K_{on}^{rand}, B, E), and mean T-cell velocities as a function of chemokinerelease rates (C) for CRMs releasing CCL21 (A–C) or CCL19 (C–E). (F) Experimental hit rates vs. receptor occupancy gradient. Dashed lines in B, E denote hit rates expected for random migration; dashed line in C denotes background velocities of T-cells inthe absence of chemokine. Experimental data are shown as mean ± SE.

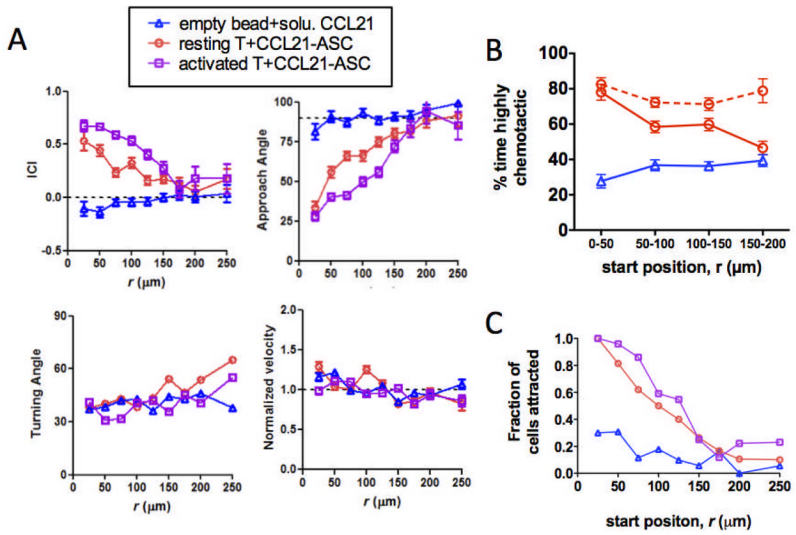

Fig. 4. CRM-generated CCL21 gradients stimulate chemotaxis of resting or activated T-cells graded by distance of the responding T-cell from the chemokine source

Resting or activated human T-cells were embedded in collagen gels at 3×10^6 cells/cm^3 with CCL21-CRMs (8×10^3 beads/cm^3, beads loaded with 7.5 μg CCL21/mg alginate) and imaged by videomicroscopy for 1.5 hr. In parallel, control samples of T-cells and empty CRMs in collagen mixed with 10 μg/mL "free" CCL21were imaged. (A) Migration parameters were calculated as averages for all individual cell displacements occurring at a given distance from the bead (binned in 25 μm intervals) over the 1.5 hr imaging time for resting T-cells (red, n = 122 cells) or activated T-cells (purple, n = 87 cells) responding to CCL21-releasing CRMs, or resting T-cells in the presence of empty beads and free CCL21 (blue, n = 61 cells). Shown are mean ± SEM for instantaneous chemotactic index (ICI), approach angle, turning angle, and normalized velocity. (B) The percentage of time-steps individual T-cells exhibited ICI values > 0.5 (% time highly chemotactic) was calculated, and shown are mean values as a function of T-cells' starting positions in the gradient. Dashed red line indicates analysis for attracted T-cells only, which migrated into contact with the CRM during the experiment. (C) Fraction of cells migrating into contact with a CRM during the observation period as a function of their starting position.

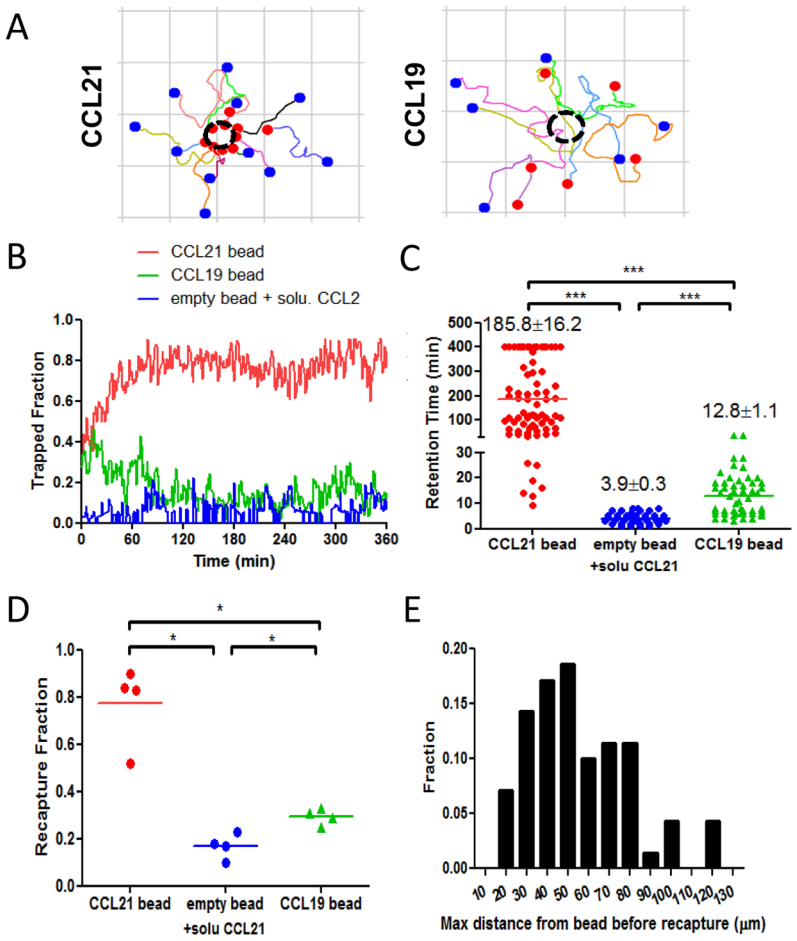

Fig. 5. Non-desensitizing CCL21 gradients elicit persistent chemotaxis and swarming of lymphocytes around isolated chemokine sources, while CCL19 gradients elicit transient cell attraction

Fields of view containing a single central CRM releasing CCL21 (7.5 μg CLL21 per mg alginate), CCL19 (1 μg CCL19 per mg alginae), or empty beads surrounded by uniform concentration of free CCL21 (10 μg/mL) were imaged over 6 hr. (A) Path plots of individual cells around CCL21- or CCL19-releasing CRMs over the first 90 min; dashed circle indicates the location of chemokine-CRMs; blue solid circle indicates the start of migration path and red solid circle indicates the end of migration path; grids are 100 μm × 100 μm.(B) The fraction of T-cells in contact with the surface of the nearby CRM over 6 hr. (C) Retention time of individual T-cells at the surface of an CRM following initial contact with the beads. (D–E) The behaviour of “escaping” cells that migrated at least 20 μm away from the bead surface against CCL21 or CCL19 gradients over 3 hr was characterized: (D) Mean frequency of escaping T-cells recaptured by the attractant gradients. (E) Histogram of maximum distance “recaptured” T-cells migrated away from CRM before turning and returning to the local chemokine source.*, $p < 0.05$; ***, $p < 0.001$.

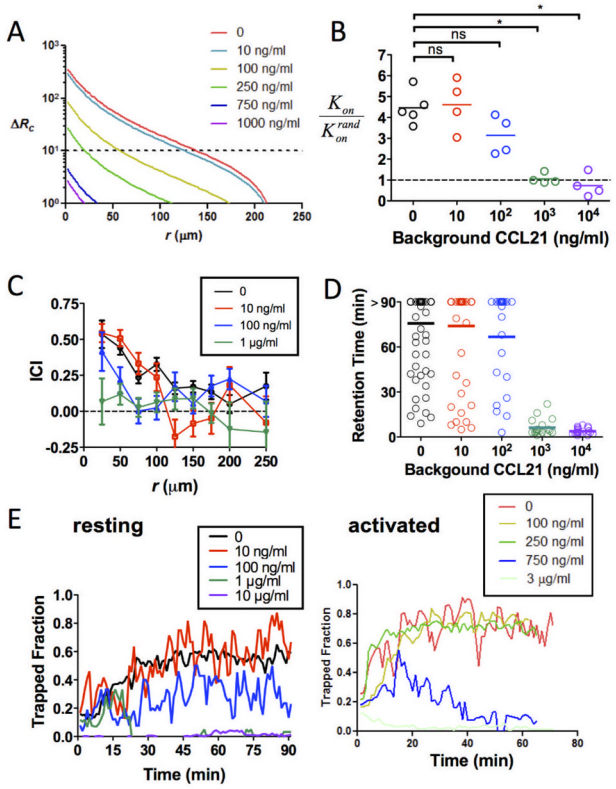

Fig. 6. Levels of ambient attractant around chemokine sources regulate migration responses to CCL21

(A) Receptor occupancy gradients at t = 30 min calculated for CCL21-CRMs ((8×10^3 beads/cm^3, 7.5 μg CCL21 per mg algiante) with surrounding ambient CCL21 concentrations varying from 10 ng/ml to 1 μg/ml as indicated. (B–D) Migration response of resting T-cells to CCL21-releasing CRMs in the presence of increasing ambient levels of CCL21 in the collagen matrix (concentrations as indicated). Shown are hit rate ratios (B), instantaneous chemotactic indices as a function of distance from the bead surfaces (C), and retention times of individual T-cells around CCL21-CRMs (D). (E) Fraction of resting T-cells (left) and activated T-cells (right) trapped around CCL21-CRMs in the presence of ambient chemokine. *, $p< 0.05$.

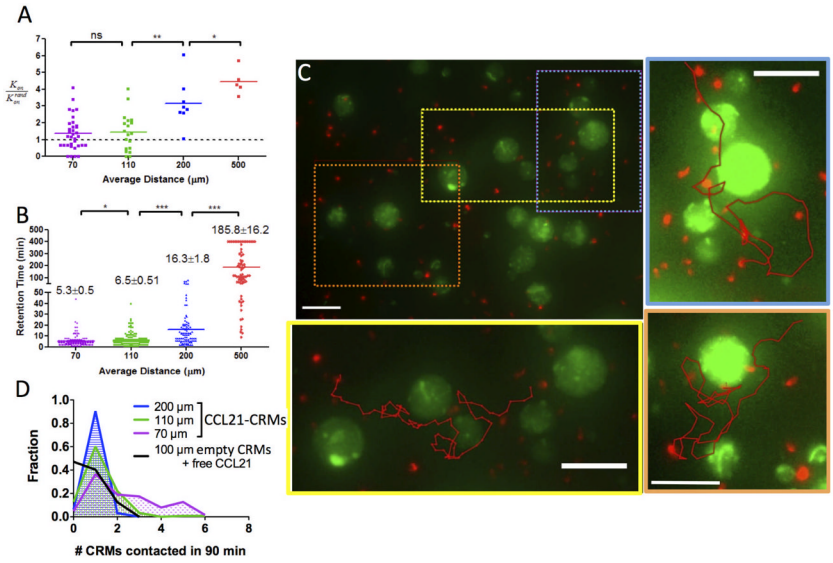

Fig. 7. Dense chemokine point sources elicit local chemoattraction and "hopping" of resting T-cells between adjacent sources

Resting human T-cells were embedded in collagen gels with CCL21-CRMs at the indicated mean center-to-center separations and imaged by videomicroscopy for 1.5 hr. (A) Hit rate of T-cells migrating into contact with individual CCL21-CRMs as a function of bead separation. (B) Retention time of cells in contact with individual microspheres. (C) Representative cell tracks illustrating how individual cells navigated among multiple CCL21-microspheres. Scale bars 50 μm. (D) Histograms of the number of distinct CRMs that single cells contact in 60 min, comparing CCL21-CRMs at varied spacing to empty CRMs in the presence of a uniform field of CCL21 (10 μg/mL). *, $p < 0.05$; **, $p < 0.01$.

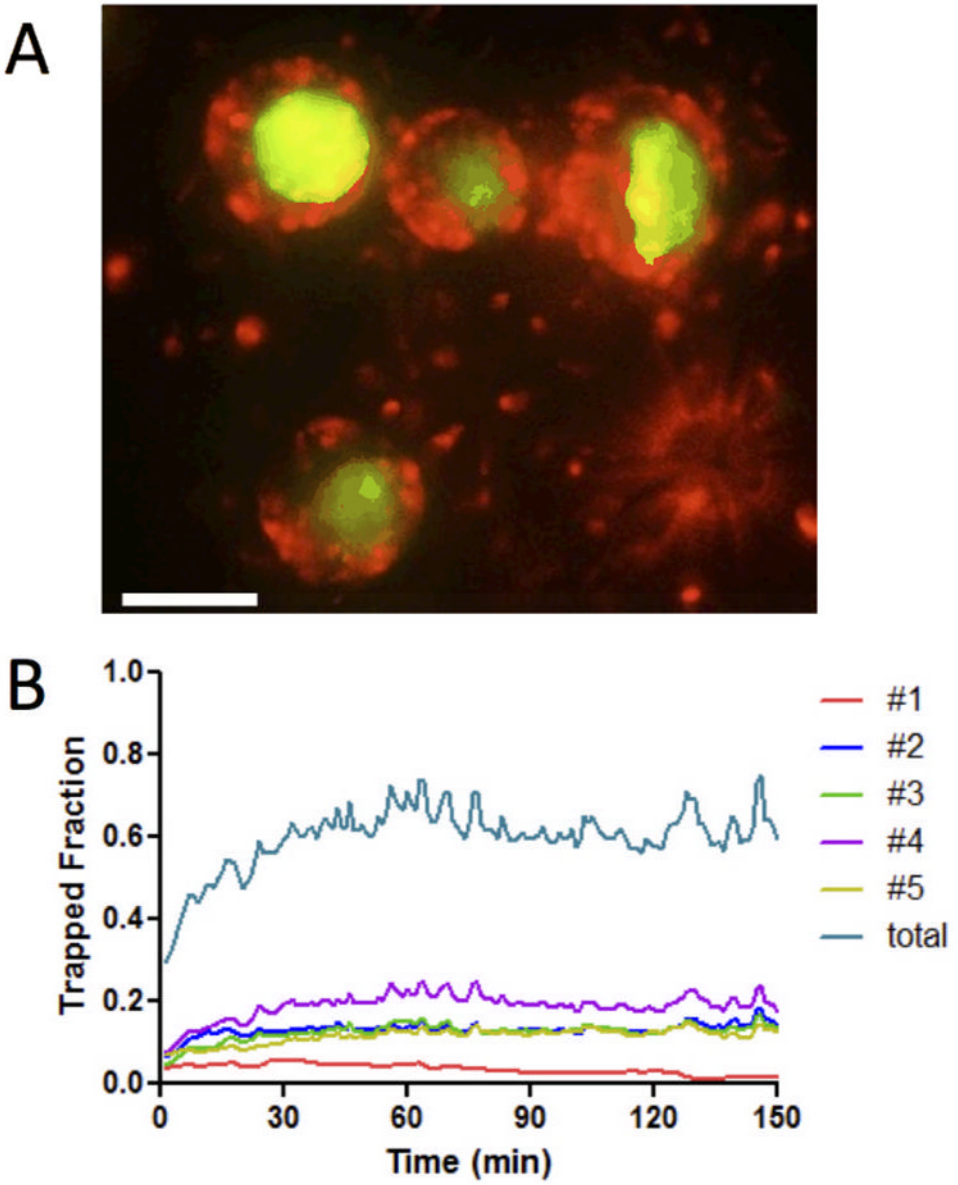

Fig. 8. Activated T-cells are trapped by weak localized gradients even in the presence of dense attractant sources

Activated human T-cells were embedded in collagen gels with CCL21-CRMs (mean bead separation 100 μm, releasing CCL21 at 0.7 pg/bead/hr) and imaged by videomicroscopy for 3 hr. (A) Representative snapshot of T-cells swarming around closely spaced beads at 30 min (red, T-cells; green, CCL21-CRMs). Scale bar 50 μm. (B) The fraction of T-cells trapped around 5 different individual beads as well as the total fraction of activated T-cells trapped around beads in one field of view over time.